ACSNANO www.acsnano.org

ARTICLE

Highly Stable and Conductive Microcapsules for Enhancement of Joule Heating Performance

Zhaoliang Zheng,[†] Jidong Jin,[‡] Guang-Kui Xu,[*,§] Jianli Zou,[†] Ulrike Wais,[†] Alison Beckett,[∥] Tobias Heil,[¶] Sean Higgins,[#] Lunhui Guan,[⊥] Ying Wang,[§] and Dmitry Shchukin[*,†]

[†]Stephenson Institute for Renewable Energy and Department of Chemistry, University of Liverpool, Liverpool L69 7ZD, United Kingdom

[‡]Department of Electrical Engineering and Electronics, University of Liverpool, Liverpool L69 3GJ, United Kingdom

[§]International Center for Applied Mechanics, State Key Laboratory for Strength and Vibration of Mechanical Structures, Xi'an Jiaotong University, Xi'an 710049, China

[∥]EM Unit, Department of Cellular & Molecular Physiology, University of Liverpool, Liverpool L69 3BX, United Kingdom

[¶]Nanoinvestigation Centre at Liverpool, University of Liverpool, Liverpool L69 3GL, United Kingdom

[#]Centre for Materials Discovery, University of Liverpool, Liverpool L69 7ZD, United Kingdom

[⊥]Fujian Institute of Research on the Structure of Matter, Chinese Academy of Sciences, Fuzhou 350002, China

Supporting Information

ABSTRACT: **Nanocarbons show great promise for establishing the next generation of Joule heating systems, but suffer from the limited maximum temperature due to precociously convective heat dissipation from electrothermal system to surrounding environment. Here we introduce a strategy to eliminate such convective heat transfer by inserting highly stable and conductive microcapsules into the electrothermal structures. The microcapsule is composed of encapsulated long-chain alkanes and graphene oxide/carbon nanotube hybrids as core and shell material, respectively. Multiform carbon nanotubes in the microspheres stabilize the capsule shell to resist volume-change-induced rupture during repeated heating/cooling process, and meanwhile enhance the thermal conductance of encapsulated alkanes which facilitates an expeditious heat exchange. The resulting microcapsules can be homogeneously incorporated in the nanocarbon-based electrothermal structures. At a dopant of 5%, the working temperature can be enhanced by 30% even at a low voltage and moderate temperature, which indicates a great value in daily household applications. Therefore, the stable and conductive microcapsule may serve as a versatile and valuable dopant for varieties of heat generation systems.**

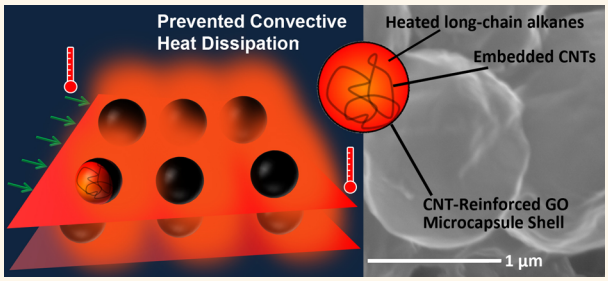

KEYWORDS: *microcapsule, ultrasound, emulsification, encapsulation, graphene oxide, carbon nanotube, nanocarbon hybrids, electrothermal*

Joule heating, generated when an electric current passes through a conductor, has been widely used in daily applications. As an emerging alternative to conventional metal-based Joule heater, nanocarbons exhibit distinguished advantages in robust electrical/thermal conductivity,[1−4] high flexibility[5,6] and mechanical strength,[7] transparency[8] and low weight.[9] Currently, there has been a burgeoning interest in employing them, for example, carbon nanotubes (CNTs),[10,11] reduced graphene oxide (RGO)[12] and graphene,[13,14] as two-dimensional (2D) flexible heating devices for mild temperature (less than 100 °C) applications. However, increasing the maximum temperature at a given voltage or input power remains challenging due to the excessively and inevitably convective heat dissipation from the electrothermal system to surrounding environment (Figure 1a). The saturated temperature was even reported to be depended on the input power and convective heat-transfer coefficient.[14] As such, decreasing the precociously convective heat transfer without the expense of conductivity, structural integrity and reliability of the

Received: February 12, 2016
Accepted: March 22, 2016
Published: March 22, 2016

DOI: 10.1021/acsnano.6b01104
ACS Nano 2016, 10, 4695−4703

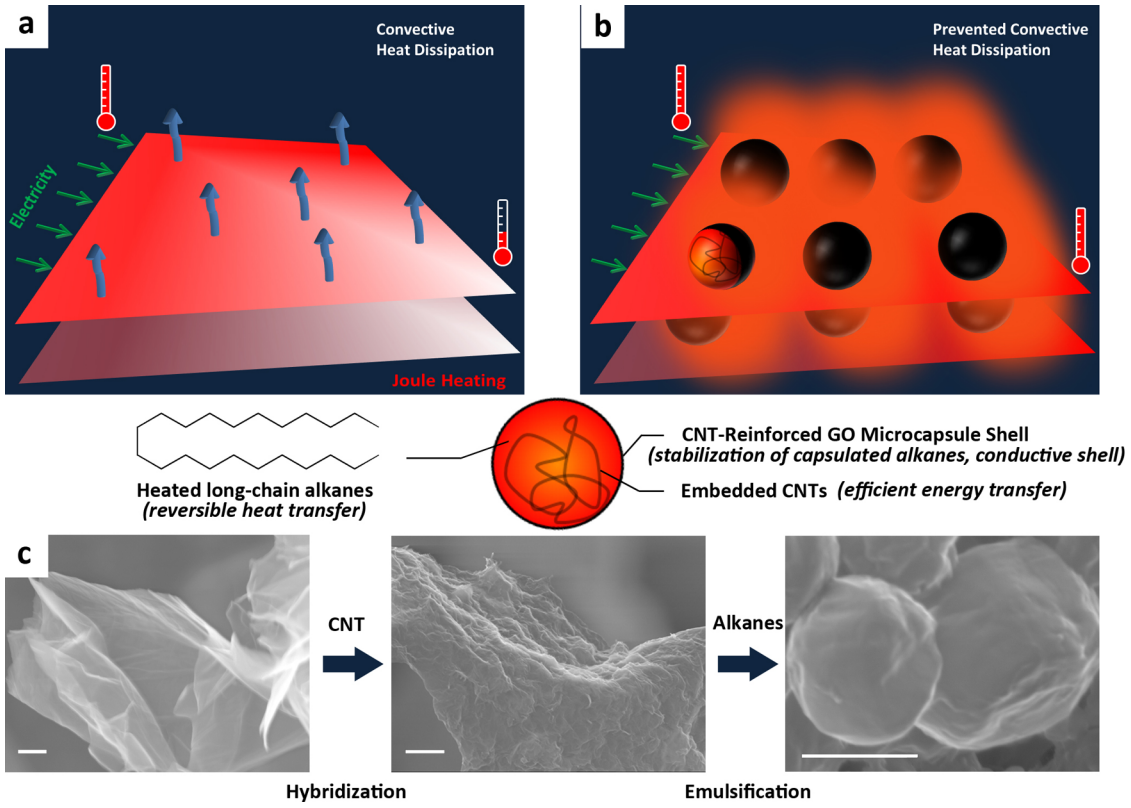

Figure 1. The role and formation process of C22@GO−CNT microcapsules. (a) The maximum temperature of Joule heater is always limited by the inevitably convective heat transfer between electrothermal system and surrounding environment. (b) C22@GO−CNT microcapsules fill the space and voids between electrothermal sheets without altering the degree of sheet orientation and alignment, and thus conserve the conductance of Joule heating system. The heat released by capsules can effectively prevent convective heat dissipation, and thus increase the maximum temperature of the Joule heater. (c) Scanning electron microscopy (SEM) images of GO sheets, GO−CNT hybrids and as-prepared C22@GO−CNT microcapsules demonstrate a facile procedure for the stable and conductive microcapsules. Scale bar: 1 μm.

electrothermal system would be the most promising way to solve the aforementioned problem. Complementation of this seemingly self-contradictory requirement is heralded as a novel and versatile platform for improving electrothermal, photothermal, magnothermal and chemothermal conversion efficiency (Figure 1b).

Due to the relatively high volumetric heat capacity (>2 J cm^{-3} K^{-1})[15] and fusion heat (>200 kJ kg^{-1}), the encapsulated long-chain alkanes (C_nH_{2n+2}, $n \geq 16$)[16] have been intensively studied for fostering rapid, sustainable and reversible heat exchange between the alkanes and environment. The design of filling up the space of air with encapsulated alkanes facilitated the realization of energy-saving buildings and temperature-regulating textiles.[17] Yet such a concept has rarely been adopted in electrothermal systems, because several intrinsic weaknesses of capsulated alkanes limited their role: (1) large volume change during melting/solidifying process may cause the shells to rupture, resulting in unstable performance responsive to the leaked alkanes;[18] (2) inherently low thermal conductivity of alkanes and traditional polymer shell decreases the heat storage and transfer efficiency;[19] and (3) low electrically conductive shells may impede electron transport through the conductive networks of electrothermal systems.

A satisfactory answer on the above questions is still pending, but the microencapsulation of alkanes (*e.g.*, Docosane, $C_{22}H_{46}$) with graphene oxide/carbon nanotubes hybrids (denoted as C22@GO−CNT) may offer a solution. In this design, amphiphilic GO nanosheets, the building blocks of Joule heating system, act as main candidates of the potentially conductive microcapsule shell.[20] *Via* strong $\pi-\pi$ interactions between basal planes, CNTs effectively reinforce the relatively flexible GO shell and thus stabilize the capsulated docosane,[21,22] as will be demonstrated below. Additional thermal transport paths within the microconfined organic matrix are constituted by embedded CNTs in docosane, which maintains an efficient energy transfer across the CNT/alkane interface.[19] Therefore, the alkanes would continuously absorb heat from conductive nanocarbon structures[23] and release to warm up the surrounding air. Doping such conductive and stable capsules as a built-in thermal protector can prevent precocious convective heat dissipation and maintain minimum conductance degradation of electrothermal structures. We believe this work will provide a reliable encapsulation technique and ease of operation for thermal energy utilization.

RESULTS AND DISCUSSION

Morphology of Microcapsules and CNTs Configurations. Figure 1c is a schematic of the formation steps involved in obtaining our stable and conductive microcapsules. In brief, the GO−CNT hybrids along with CNT clots (as shown later in Figure 2j) were formed under pulsed tip-sonication and then directly applied in the following ultrasound-induced emulsification with melted C22, which resulted in C22@GO−CNT microcapsules. At the emulsification step, the CNT-hybridized GO sheets assemble at the oil/water interface to stabilize the encapsulated docosane;[20] simultaneously the CNT clots are

DOI: 10.1021/acsnano.6b01104
ACS Nano 2016, 10, 4695−4703

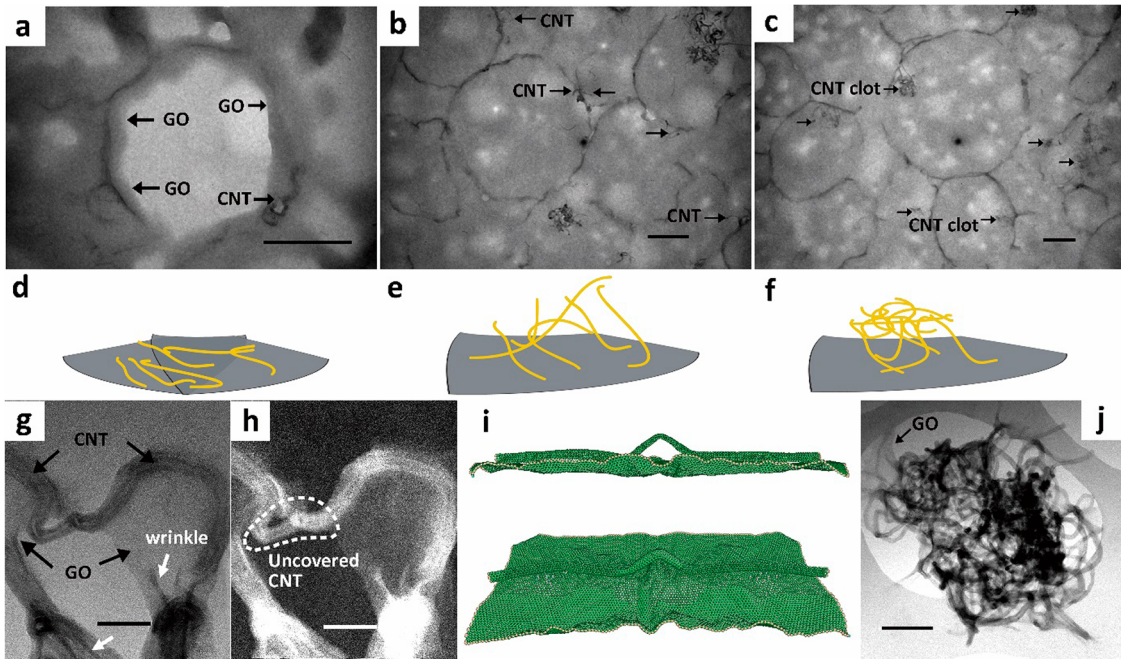

Figure 2. Structural and morphological characterization of C22@GO−CNT microcapsules. Transmission electron microscopy (TEM) images of ultrathin sections from ultramicrotomy showing (a) the CNTs are completely adhered on GO layers, (b) partially adhered and partially inward extended, and (c) even led to clots embedded in C22, respectively. (d−f) Schematic models of the three configurations of CNTs within C22@GO−CNT microcapsules. The gray lamellar and yellow wires represent the GO sheet and CNTs, respectively. TEM images of GO−CNT hybrids in bright field imaging mode (g) and high-angle annular dark-field imaging mode (h) are shown. Individual CNT covered by GO sheets is demonstrated, with some uncovered parts (white dashed circle) and wrinkled structures (white arrows) detected. Molecular dynamics simulation of the "GO−CNT" assembly show side view (i, top) and tilted top view (i, bottom) of a snapshot during the relaxation process. The wire-like nanotube and silk-like GO can be distinguished. Additionally, a CNT clot (j) is adhered by GO sheets. Scale bar: (a−c) 500 nm; (g and h) 50 nm; (i) 5 nm; (j) 200 nm.

embedded in the oil phase. The C22/GO/CNT weight ratio can be tailored by changing the concentration of GO aqueous dispersion and amount of CNTs during the GO−CNT hybridization. The alkanes can also be extended to other candidates (n = 16, 18, and 20, Figure S1). We show the narrowly size-distributed C22@GO−CNT microcapsules prepared with the C22/GO/CNT weight ratio of 500/10/0.2 in Figure S2. They exhibit a smaller size (1.3 ± 0.3 μm) as compared with the ones of emulsions stabilized only by GO or acidified CNT: C22@GO and C22@CNT (500/10/0, 6.9 ± 1.9 μm; 500/0/10, 2.6 ± 0.6 μm). In contrast to other GO-based leakage-preventing capsules which were formed *via* similar emulsion process,[24−26] the C22@GO−CNT microcapsules are 1 to 2 orders of magnitude smaller. It is mainly q result from the synergistic effect between GO and CNT that accounts for compensating the large pressure induced from such small and highly curved droplets.[27] Raman spectrum of C22@GO−CNT changes little at GO characteristic peaks at D (~1350 cm^{-1}), G-bands (~1600 cm^{-1}),[28] C−H stretching mode[29] (from alkane) and D/G intensity ratio (1.4), as compared with C22@GO (Figure S3). However, the 2D-band intensifies to >2.5 times and is broadened toward that of pristine CNTs (2700 cm^{-1}), which confirms the presence of CNTs within the capsules.

Detailed observations at the sections of ultramicrotomed C22@GO−CNT unclosed the multiform CNTs in microcapsules: completely horizontal adherence on GO layers (Figure 2a,d), partial adherence and partial inward extension (Figure 2b,e), and clot attached to the inner wall of capsules (Figure 2c,f). The heterogeneous configurations of CNTs within the microcapsules will be discussed later in this paper. Upon removal of encapsulated C22 and the topside of some capsules, such randomly distributed configurations could be further confirmed in Figure S4 where the multiform CNTs were located mainly in void spaces of original encapsulated alkanes. On the basis of the experiment result, the length of CNTs ranges from to tens of nanometers to a few micrometers, but a preferable configuration of them inside microcapsules was not available, as we have adjusted GO/CNT weight ratio at 10/0.01, 10/0.1, 10/0.2, and 10/1 (not shown here). Comparison of the energy required for completely horizontal adherence on GO (E_{CNT-GO}) and perfect embedment within C22 ($E_{CNT-C22}$) supports the observation, yet also reveals the short CNT is more likely completely adhered by GO *via* $\pi-\pi$ interaction,[21,22] whereas the long one prefers interaction with C22 (Supporting Information Note 1).

Evidence is shown that the multiform CNTs in microcapsules originate from the ultrasound-assisted hybridization of nanocarbons. The ultrasonic treatment of GO and CNT mixture leads to the adherence of CNTs on GO sheets and random-oriented wrinkled structure which can be discovered in magnified images (Figure 1c and Figure S5). The adherence process was detected by tracking the blue shift of GO C═C stretching vibration absorption (from 1642 cm^{-1}) with time (Figure S6). The shift suggests an enhanced electron delocalization, in other words, a more compact $\pi-\pi$ stacking structure formed between GO and CNT.[30] After 15 min, the ultrasound-assisted assembly was believed to reach a saturated state because the peak was fixed at 1623 cm^{-1}. Figure 2g shows that the aromatic conjugation helps in the formation of "GO−

DOI: 10.1021/acsnano.6b01104
ACS Nano 2016, 10, 4695−4703

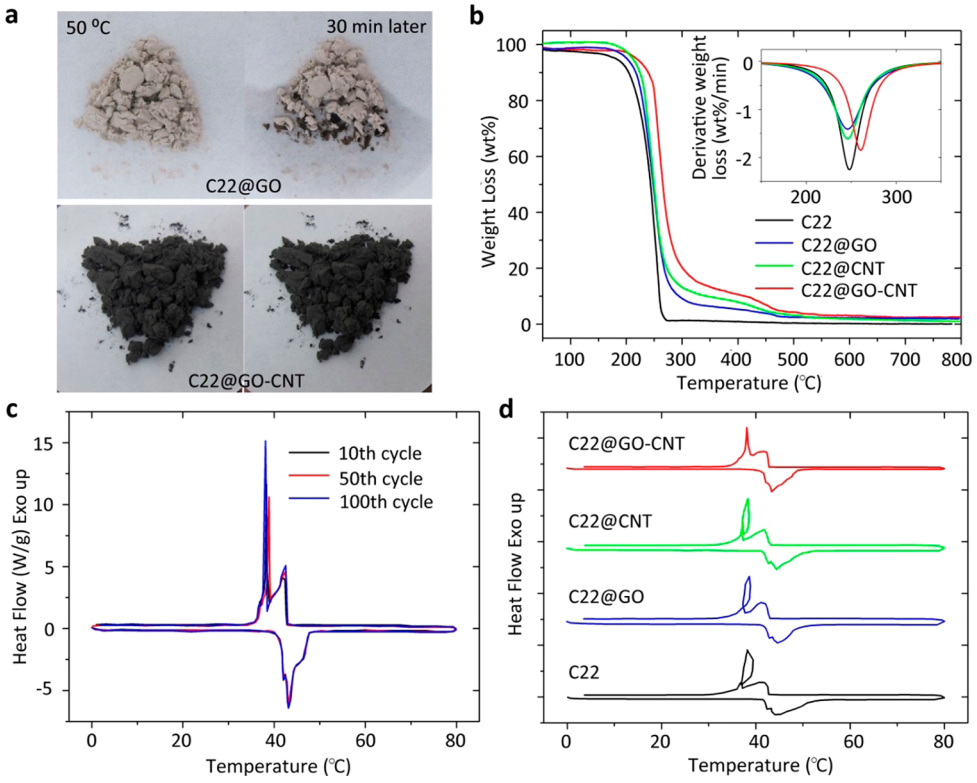

Figure 3. Thermal stability measurement of microcapsules. (a) At duration of 30 min, the shape changes of C22@GO and C22@GO−CNT at around 50 °C are shown. No detectable leakage was observed for C22@GO−CNT capsules. TG (b) and DTG (inset) curves of bulk C22, C22@GO, C22@CNT, and C22@GO−CNT are demonstrated. The TG curve of C22@GO−CNT in decreasing process exhibits two-step weight loss that, respectively, corresponds to decomposition of alkanes (200−300 °C) and degradation of carbon shells (400−500 °C). A postponed decomposition was obvious by comparing with other samples. DSC curves (c) of C22@GO−CNT at 10th, 50th, and 100th thermal cycle were obtained at the rate of 5 °C/min. During the measurement, the melting and crystallizing points varied slightly. DSC curves (d) of bulk C22, C22@GO, C22@CNT, and C22@GO−CNT at the rate of 10 °C/min are displayed. The subcooling circle, delayed structural change, happens at C22@GO, C22@CNT, and bulk C22 in between 37 and 40 °C.[49,50]

CNT" assemblies by covering the surface of an individual CNT by one side of GO layers,[31,32] which contributes to the horizontal adherence of CNTs on GO layers. On the basis of the image, the width of wrinkles can also be estimated to be 3−5 nm. In comparison, the sonicated GO sheets without CNTs only possess wrinkles wider than 200 nm (Figure S7). As such, the adherent CNTs are likely to induce the buckling effect on the basal plane of GO. If the CNTs are shorter than the persistence length (about 200 nm),[33] they behave as a rod and completely adhere on GO layer (Figure 2d). It is difficult to bend them because the bending energy is large enough to prohibit their peeling off from the GO layer. From the view of GO layers, the bending stiffness can be expressed as[34]

$$B = Et^3/[12(1 - \nu^2)] \quad (1)$$

where B is the bending stiffness of the GO layer, E is the Young's modulus of the GO layer, and ν is the Poisson's ratio. For monolayer GO that interacts with CNTs, the Young's modulus E is around 200 GPa, and the thickness t is 0.7 nm.[35] The exact value of Poisson's ratio is not known, but can be supposed to be 0.165 as the value for graphite in the basal plane.[36] Thus, the adhesion strength of CNT on wrinkled GO layers can be calculated as[37]

$$F = \pi^2 Bt/L \quad (2)$$

where L is the width of wrinkle (5 nm, Figure 2g). Using these values, one can estimate F is in the order of 10^{-9} N. If the layer has been compressed a few nanometers, the work W done by this force is in the order of 10^{-18} J, which is in agreement with the reported effective adhesion energy between CNT and GO (−500 kJ/mol).[38] As such, the CNT-hybridized GO shells are reinforced at a planar direction,[39] resulting in highly stable encapsulated alkanes in the following repeated melting/solidifying process.

Meanwhile, the uncovered CNT can be detected adjacent to the covered ones (Figure 2h). It holds a great possibility for this part to form the second configuration of CNTs during the emulsification. In addition, we conducted molecular dynamics simulation of the "GO−CNT" assembly to probe the forming mechanism of the heterogeneous configuration of CNTs on GO sheets (Figure 2i). Indeed, the relaxation process reveals that the aromatic conjugation can only allow CNTs to be partially adhered on wrinkled GO basal planes, which is in good agreement with the experimental observation. The partial coverage is common among the CNTs longer than the persistence length; they are modeled as semiflexible chain with configuration of partially adhering on GO layer and partially penetrating into the interior (Figure 2e).[40] In this case, it is difficult to fix them totally on GO because they tend to occupy more space to obtain larger configurational entropy. In addition, CNT clots with averaged diameter as large as 600 nm were also found, even at a lower (10/0.01) or higher (10/1) weight ratio (Figure S8). GO layers only catch them by adhering on a limited numbers of peripheral CNTs (Figure 2j).

DOI: 10.1021/acsnano.6b01104
ACS Nano 2016, 10, 4695−4703

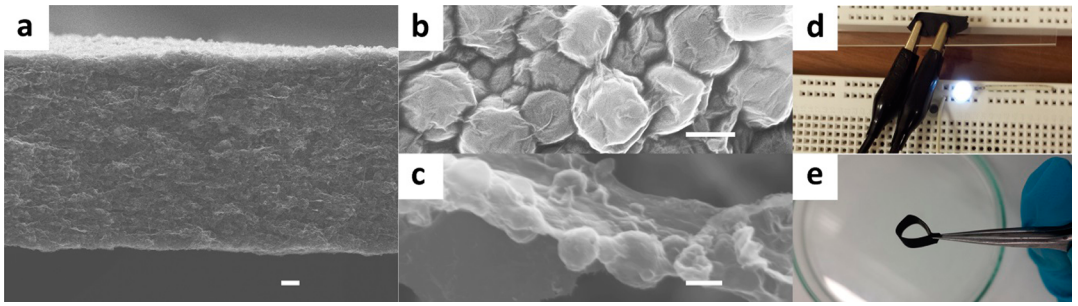

Figure 4. Planar C22@GO−CNT/GO composites. (a) SEM image of cross sections of free-standing planar composites is shown. The composite was made up by vacuum filtrating aqueous mixture containing 25% of C22@GO−CNT microcapsules and 75% GO in concentration. The top-view of the composite (b) shows the microcapsules fully covered by GO sheets. Several layers were stripped off the planar 25-C22@GO−CNT/GO. (c) High-resolution SEM shows the capsules are embedded at basal plane of GO sheets, resulting in a "built-in" structure. (d) An LED lamp was illumined when r25-C22@GO−CNT/GO was connected between clips. And so were the other composite containing 0−100% C22@GO−CNT microcapsules. (e) A rC22@GO−CNT/GO composite remains flexible when the C22@GO−CNT concentration is below 50%. Scale bar: (a) 10 μm; (b and c) 1 μm.

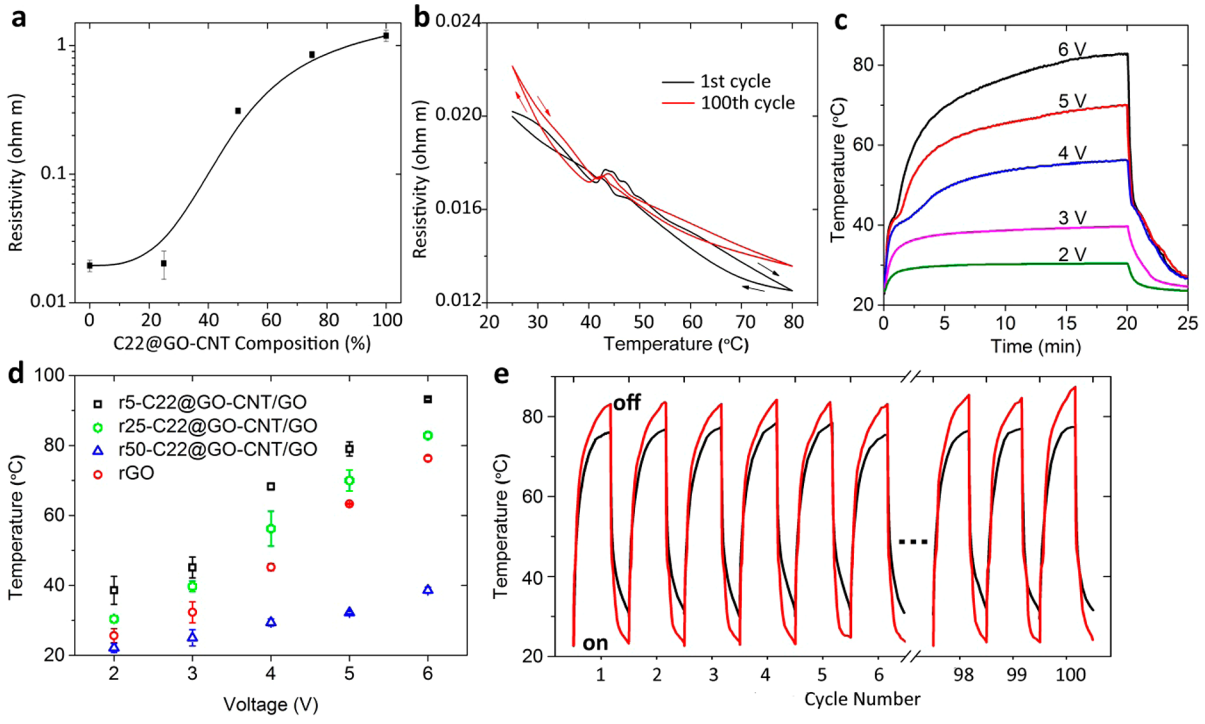

Figure 5. Electrical conductivity and electrothermal performance of rC22@GO−CNT/GO composites. (a) The resistivity of rC22@GO−CNT/GO composite varies with the volume concentration of C22@GO−CNT. (b) As a function of temperature, the resistivity curves of the 1st and 100th thermal cycles change slightly, indicating the conductive structure is stable. (c) Temperature evolution curves of r25-C22@GO−CNT/GO under constant voltages of 2, 3, 4, 5, and 6 V. (d) As a function of voltage, the balanced surface temperatures obtained at 20 min heating are demonstrated. The samples of r5-C22@GO−CNT/GO, r25-C22@GO−CNT/GO, 50-C22@GO−CNT/GO, and neat rGO heater were studied. (e) A collection of temperature evolution curves of r25-C22@GO−CNT/GO composite and neat rGO heater under 6 V repeated for 100 cycles.

CNT clot, a self-aggregated assembly, is highly undesirable and causes difficulties in solution processing[41,42] but, if handled properly, would be beneficial in enhancing heat transfer efficiency within the microcapsules.

Stability and Heat Transfer of C22@GO−CNT. By introducing GO−CNT hybrids in emulsification, the C22@GO−CNT microcapsules show a distinguished stability. As depicted in Figure 3a and Figure S9, the original shape of C22@GO−CNT solid powder was retained at the temperature higher above the melting point of docosane, whereas the unprotected docosane deformed into liquid quickly, and there was also obvious leakage from C22@GO and C22@CNT capsules. More details about the thermal stability of microencapsulated alkanes were examined with thermogravimetric (TG) and derivative TG (DTG) analyses. Figure 3b presents that docosane mass percentage of C22@GO−CNT is maintained at around 80%, which is slightly lower than that of the other two kinds of microcapsules. However, DTG curves (inset Figure 3b) demonstrate that the thermal stability of alkanes can be improved by microencapsulating in the hybridized shell because C22@GO−CNT exhibits the highest temperature (260 °C) of maximum weight loss rate. Furthermore, differential scanning calorimetry (DSC) was employed to confirm that there is little change in C22@

DOI: 10.1021/acsnano.6b01104
ACS Nano 2016, 10, 4695−4703

GO−CNT thermal properties after 100 thermal cycles (Figure 3c). The average latent heats of docosane have remained around 240.8 J/g, leading to an encapsulation ratio of alkane as high as 96.7% by comparing with the enthalpy of bulk state.[43] As far as we know, it is the highest value comparing with other reported microencapsulated alkanes,[26] indicating a timely and sufficient structural change of C22 in response to temperature change. Figure 3d also confirms this by unveiling no notable subcooling circle of C22@GO−CNT even at a high cooling rate (10 °C/min). Subcooling is common among the low thermal conductive materials where solidification occurs below its melting temperature.[44] The effect of confinement can be ruled out because the sizes of the examined capsules are all at range of 1−10 μm. Although the interfacial thermal conductance[45] between alkane and CNT is relatively low due to the large mismatch in phonon spectra,[46] the embedment of individual and clot-shaped CNTs can enhance the heat transfer within the microcapsules and provides nucleation sites for crystallization by molecular interaction.[19]

Fabrication of Planar C22@GO−CNT/GO Composites. The high ζ-potential of C22@GO−CNT microcapsules at around −46 mV ensures a homogeneous distribution in constructing C22@GO−CNT-doped composites. Aside from this dispersibility, C22@GO−CNT can resist a high pH value even at 7 and maintain the stability of emulsion shape (Figure S10), which is easily understood as reinforcing role of CNTs on GO shell to neutralize the pH-induced increase of hydrophilicity.[20,26,47] Next, vacuum filtration of colloidal dispersions of GO and C22@GO−CNT microcapsules yielded free-standing planar C22@GO−CNT/GO composites with tailored thickness and composition, denoted as *x*-C22@GO−CNT/GO where *x* represents percentage volume concentration of the microcapsules in colloidal dispersions (Figure 4a and Figure S11). A top-view of 25-C22@GO−CNT/GO reveals the wrinkled but closely packed GO layers fully cover the capsules (Figure 4b). Meanwhile, some stripped-off layers of 25-C22@GO−CNT/GO unveil that the capsules are embedded at basal plane of GO sheets (Figure 4c). The GO simultaneously as shell materials of capsule and building blocks of electrothermal system enables C22@GO−CNT to homogeneously dope, resulting in the "built-in" structure. After reduction, an LED can be illumined at 1.8 V when connected with the reduced planar composites (Figure 4d). Moreover, the evenly doped structure renders the reduced 25-C22@GO−CNT/GO (r25-C22@GO−CNT/GO) composite an almost intact flexibility as compared with the undoped one (Figure 4e), which cannot be obtained by the conventional composites of solid alkanes and nanocarbons.[48]

Joule Heating Performance of Reduced C22@GO−CNT/GO Composites. The completely encapsulated alkanes have little effect on the overall conductance of the Joule heating system in the repeated melting/solidifying process. As shown in Figure 5a, the electrical resistivity of the r*x*-C22@GO−CNT/GO composites with dopant below 25% remains 2.0×10^{-2} Ω·m at 25 °C. This indicates a threshold doping value for incorporating our microcapsules without disturbance of conductive pathway of GO sheets (Figure 1b). As a function of temperature, the electrical resistivity of all reduced composites demonstrated the steadily decrease (by less than 2 times) as the temperature was increased to 80 °C, and recovered when the composites were cooled down (Figure S12). Notably, there are only weak peaks observed during the phase transition of docosane (42−46 °C). Beyond the phase transition region, the conductive structure of the composites was stabilized, and thus, less change in electrical resistivity was detected. In comparison, a graphite/hexadecane mixture without encapsulation was reported to have a 2 orders of magnitude change of conductivity due to the internal stress generated during the phase change.[18] Furthermore, r25-C22@GO−CNT/GO demonstrates similar temperature-dependent electrical resistivity curves at the first and 100th thermal cycle (Figure 5b), suggesting an excellent thermal stability within the range of expected working temperatures.

Being exposed to air (22 °C) and subjected to convective heat dissipation, r*x*-C22@GO−CNT/GO composites were examined for surface temperature evolution under voltage of 2, 3, 4, 5, and 6 V (Figure 5c). In comparison with neat rGO, r25-C22@GO−CNT/GO composite exhibits the enhanced maximum temperature of 30.4, 39.7, 56.2, 70, and 82.8 °C with increased voltage (Figure S13). The maximum temperature can be further improved by generally 30% through decreasing the dopant to 5% in our recent system (Figure 5d and Figure S14).). This means the microcapsules quickly balance the temperature discrepancy with heating source and release heat to environment, even at moderate temperature. It has a great value in mild-temperature applications, for example, incubation, planting and brewing. Finally, the heating and cooling processes of r25-C22@GO−CNT/GO composite under high voltage value can be repeated for 100 cycles without notable degradation (Figure 5e and Figure S15). The composite maintains an around 10% enhancement in maximum temperature. Regarding the encapsulated alkanes, evidence is shown with r25-C22@GO−CNT/GO composite (Figure 5c) where phase change regions of docosane can be clearly distinguished when the temperature is heated up above the melting range. We prepared a control sample by removing docosane from r25-C22@GO−CNT/GO composite (Figure S16). Now, the sample possesses a comparable supporting framework and electrical conductivity (1.9×10^{-2} Ω·m) as r25-C22@GO−CNT/GO but only slightly enhances the maximum temperature as compared with neat rGO (Figure 5d). At the confined space within the hybridized capsule shell, alkanes act as heat reservoir with capacity 3 orders of magnitude higher than air (1.2×10^{-3} J cm^{-3} K^{-1}). As such, more heat can be simultaneously accumulated and released to eliminate the convective heat dissipation.

CONCLUSIONS

A novel strategy for the elimination of precociously convective heat dissipation from electrothermal system using highly stable and conductive encapsulated long-chain alkanes was demonstrated. The traditional well-encapsulated long-chain alkanes always required the formation of thick polymer shell[26] which would mitigate the energy transfer efficiency by a retarded thermal/electrical conductance. In our design, the multiform CNTs within the GO−CNT hybridized microcapsules can maintain the integrity of encapsulation during the repeated heating/cooling process, and meanwhile facilitate the quick heat exchange between the microconfined alkanes and environment. As such, a combination of multiple advantages is realized in one single capsule which sets our work apart from previous microcapsules for heat utilization. The work is virtually applicable to a wide variety of organic molecules that can be encapsulated in our hybridized nanocarbon shell, opening new avenues for approaching the targeted performance by selecting materials with different heat capacity and thermal conductance.

DOI: 10.1021/acsnano.6b01104
ACS Nano 2016, 10, 4695−4703

With the application of our microcapsules, exciting opportunities may arise from enhancing solar-heat transfer efficiency at regions lacking sunlight, for example, northwest England. In addition, given the unique existence of multiform CNTs, the underlying principle and more derived complex structures hold great promise for smart heater and signal transmitter spanning multiple length scales.

METHODS

GO−CNT Hybridization and Ultrasound-Induced Emulsification for C22@GO−CNT Microcapsules. For C22@GO−CNT microcapsules (C22/GO/CNT = 500/10/0.2), 5 mL of GO aqueous solution (2 mg/mL) was tuned by chloride acid to pH = 2, followed by adding 0.2 mg of MWCNTs. The sonicator probe end was placed just below the surface of the liquid (about 0.5 cm into solution), and the mixture was pulse-sonicated (Model Q700, 20 kHz; Qsonica) for 10 min (amplitude: 30%, 5 s on, 5 s off) in open environment with a 1.8 cm diameter titanium probe (model BS 2d18F). Upon completion of sonication, the temperature of reaction mixture may reach around 60−70 °C. Then, 500 mg of docosane was added directly onto the as-prepared GO−CNT hybrids dispersion. The temperature was maintained at around 45 °C until the docosane was completely melted. Then, the sonicator probe end was placed at the interface of docosane and water, and the mixture was continuously sonicated for 3 min (amplitude: 30%, ∼1000 J). During the sonication process, the reaction temperature was maintained at around 45 °C by circulated water. Upon completion of sonication, the reaction product was cooled by ice−water mixture and stored in room temperature for following applications. The as-prepared emulsions remained stable for more than 2 months without any evidence of leakage (Figure S1).

Characterization. SEM analysis was conducted using a JSM-7001F Scanning Electron Microscope from JEOL. GO−CNT hybrids were investigated using a JEOL 2100FCs with a Schottky Field Emission Gun TEM (200 kV accelerating voltage). For ultramicrotomy, samples were embedded in LR White Acrylic Resin (TAAB L012/L010) and cold cured in either an embedding mold or gelatin capsules. Ultrathin section (70−80 nm) were cut on a Leica UC6 and viewed at 120 kV in a FEI Tecnai G2 Spirit. Raman spectra were measured by the Renishaw InVia Raman microscope with a 532 nm laser, a 50× objective lens and 1 mW (0.5%) as incident laser. TG and DTG use a microbalance model STA PT1000 from Linseis where the samples were heated at 5 °C/min from 25 to 800 °C in a stream of N_2. DSC was conducted using a calorimeter model Q20 from TA Instruments. Normally, samples were heated and cooled at 5 °C/min from 0 to 80 °C in a sealed nitrogen atmosphere. For fast thermal scan, the heat and cool rate could be up to 10 °C/min. The resistivities of the planar composites were investigated using a semiconductor parameter analyzer (Agilent B1500). A four-point (Van Der Pauw) configuration was used to determine the resistivity of the film from 25 to 80 °C. To characterize electrothermal performance, a thermal sensor (VR105864, Vernier) was adhered on the surface of a Joule heater to measure the temperature change. Temperature variation of the sample was recorded by a data acquisition system (LabQuest2) through the connected thermal resistor and transmitted to personal computer. The composites were connected to two copper sheets along the flat direction using conductive silver glue to ensure good contact between the composites and copper electrodes. The samples typically had areas of 5 × 5 mm^2. A workstation (Keithley 2400 Soucemeter) was linked to the samples through copper electrodes. The samples were directly exposed to environment. A variety of potentials generated from the workstation were applied to the sample for about 20 min to enable temperature increase. Electro-to-heat testing cycles were performed by applying and removing the voltage (2, 3, 4, 5, and 6 V) repeatedly at about 30 min for each cycle.

ASSOCIATED CONTENT

Supporting Information

The Supporting Information is available free of charge on the ACS Publications website at DOI: 10.1021/acsnano.6b01104.

Fabrication procedure and characterization; energy calculation and analysis; the stable emulsions for long-chain alkanes; SEM images of as-prepared C22@GO−CNT, C22@GO, and C22@-CNT microcapsules; the Raman spectra of C22@GO and C22@GO−CNT; direct observation of CNT configurations; structural characterization of GO−CNT hybrids; IR showing the hybrid structure between GO and CNT formed; SEM image of GO sheets after ultrasound treatment; the shape-stability of C22 and C22@ CNT; the pH resistance of C22@GO−CNT microemulsions; thickness of C22@GO−CNT composites increasing with C22@GO−CNT volume concentration; electrical resistivity curve of rC22@GO−CNT/GO composites; electrothermal performance of neat rGO Joule heater; electrothermal performance of r25-C22@GO−CNT composite; SEM image of the sample without docosane (PDF)

AUTHOR INFORMATION

Corresponding Authors

*E-mail: d.shchukin@liverpool.ac.uk.

*E-mail: guangkuixu@mail.xjtu.edu.cn.

Author Contributions

Z.Z. performed the all the experiments, interpreted the data, and wrote the manuscript; J.J. contributed the electrical characterization; U.W. helped with freeze-drying process; J.Z. and L.G. supported with the GO and CNT materials; A.B. contributed the ultramicrotomy and relevant TEM observation; T.H. helped with all the microscopy results; S.H. supported with the DSC measurement; Y.W. contributed with MD simulation. G.-K.X. conceived the discussion part; D.S. supervised the complementation of the project.

Funding

This work was supported by the ERC ENERCAPSULE grant.

Notes

The authors declare no competing financial interest.

REFERENCES

(1) Javey, A.; Guo, J.; Wang, Q.; Lundstrom, M.; Dai, H. Ballistic Carbon Nanotube Field-Effect Transistors. *Nature* **2003**, *424*, 654−657.

(2) Geim, A. K.; Novoselov, K. S. The Rise of Graphene. *Nat. Mater.* **2007**, *6*, 183−191.

(3) Pop, E.; Mann, D.; Wang, Q.; Goodson, K.; Dai, H. Thermal Conductance of an Individual Single-Wall Carbon Nanotube above Room Temperature. *Nano Lett.* **2006**, *6*, 96−100.

(4) Balandin, A. A.; Ghosh, S.; Bao, W.; Calizo, I.; Teweldebrhan, D.; Miao, F.; Lau, C. N. Superior Thermal Conductivity of Single-Layer Graphene. *Nano Lett.* **2008**, *8*, 902−907.

(5) Lee, C.; Wei, X. D.; Kysar, J. W.; Hone, J. Measurement of the Elastic Properties and Intrinsic Strength of Monolayer Graphene. *Science* **2008**, *321*, 385−388.

(6) Ruiz-Vargas, C. S.; Zhuang, H. L. L.; Huang, P. Y.; van der Zande, A. M.; Garg, S.; McEuen, P. L.; Muller, D. A.; Hennig, R. G.; Park, J. Softened Elastic Response and Unzipping in Chemical Vapor Deposition Graphene Membranes. *Nano Lett.* **2011**, *11*, 2259−2263.

(7) Qian, D.; Wagner, G. J.; Liu, W. K.; Yu, M.-F.; Ruoff, R. S. Mechanics of Carbon Nanotubes. *Appl. Mech. Rev.* **2002**, *55*, 495−533.

DOI: 10.1021/acsnano.6b01104
ACS Nano 2016, 10, 4695−4703

(8) Nair, R. R.; Blake, P.; Grigorenko, A. N.; Novoselov, K. S.; Booth, T. J.; Stauber, T.; Peres, N. M. R.; Geim, A. K. Fine Structure Constant Defines Visual Transparency of Graphene. *Science* **2008**, *320*, 1308−1308.
(9) Sun, H. Y.; Xu, Z.; Gao, C. Multifunctional, Ultra-Flyweight, Synergistically Assembled Carbon Aerogels. *Adv. Mater.* **2013**, *25*, 2554−2560.
(10) Kim, D.; Lee, H.-C.; Woo, J. Y.; Han, C.-S. Thermal Behavior of Transparent Film Heaters Made of Single-Walled Carbon Nanotubes. *J. Phys. Chem. C* **2010**, *114*, 5817−5821.
(11) Jang, H. S.; Jeon, S. K.; Nahm, S. H. The Manufacture of a Transparent Film Heater by Spinning Multi-Walled Carbon Nanotubes. *Carbon* **2011**, *49*, 111−116.
(12) Tan, L.; Zeng, M.; Wu, Q.; Chen, L.; Wang, J.; Zhang, T.; Eckert, J.; Rümmeli, M. H.; Fu, L. Direct Growth of Ultrafast Transparent Single-Layer Graphene Defoggers. *Small* **2015**, *11*, 1840−1846.
(13) Kang, J.; Kim, H.; Kim, K. S.; Lee, S.-K.; Bae, S.; Ahn, J.-H.; Kim, Y.-J.; Choi, J.-B.; Hong, B. H. High-Performance Graphene-Based Transparent Flexible Heaters. *Nano Lett.* **2011**, *11*, 5154−5158.
(14) Bae, J. J.; Lim, S. C.; Han, G. H.; Jo, Y. W.; Doung, D. L.; Kim, E. S.; Chae, S. J.; Huy, T. Q.; Luan, N. V.; Lee, Y. H. Heat Dissipation of Transparent Graphene Defoggers. *Adv. Funct. Mater.* **2012**, *22*, 4819−4826.
(15) Freund, M.; Mózes, G. *Paraffin Products: Properties, Technologies, Applications*; Elsevier Scientific, 1982.
(16) Arora, A. *Hydrocarbons (Alkanes, Alkenes and Alkynes)*; Discovery Publishing House Pvt. Limited, 2006.
(17) Jamekhorshid, A.; Sadrameli, S. M.; Farid, M. A Review of Microencapsulation Methods of Phase Change Materials (PCMs) as a Thermal Energy Storage (TES) Medium. *Renewable Sustainable Energy Rev.* **2014**, *31*, 531−542.
(18) Zheng, R.; Gao, J.; Wang, J.; Chen, G. Reversible Temperature Regulation of Electrical and Thermal Conductivity Using Liquid−Solid Phase Transitions. *Nat. Commun.* **2011**, *2*, 289.
(19) Chen, L.; Zou, R.; Xia, W.; Liu, Z.; Shang, Y.; Zhu, J.; Wang, Y.; Lin, J.; Xia, D.; Cao, A. Electro- and Photodriven Phase Change Composites Based on Wax-Infiltrated Carbon Nanotube Sponges. *ACS Nano* **2012**, *6*, 10884−10892.
(20) Kim, J.; Cote, L. J.; Kim, F.; Yuan, W.; Shull, K. R.; Huang, J. Graphene Oxide Sheets at Interfaces. *J. Am. Chem. Soc.* **2010**, *132*, 8180−8186.
(21) Guldi, D. M.; Rahman, G. M. A.; Jux, N.; Balbinot, D.; Hartnagel, U.; Tagmatarchis, N.; Prato, M. Functional Single-Wall Carbon Nanotube Nanohybrids Associating SWNTs with Water-Soluble Enzyme Model Systems. *J. Am. Chem. Soc.* **2005**, *127*, 9830−9838.
(22) Tung, V. C.; Huang, J.-H.; Tevis, I.; Kim, F.; Kim, J.; Chu, C.-W.; Stupp, S. I.; Huang, J. Surfactant-Free Water-Processable Photoconductive All-Carbon Composite. *J. Am. Chem. Soc.* **2011**, *133*, 4940−4947.
(23) Eda, G.; Fanchini, G.; Chhowalla, M. Large-Area Ultrathin Films of Reduced Graphene Oxide as a Transparent and Flexible Electronic Material. *Nat. Nanotechnol.* **2008**, *3*, 270−274.
(24) Yuan, K. J.; Wang, H. C.; Liu, J.; Fang, X. M.; Zhang, Z. G. Novel Slurry Containing Graphene Oxide-Grafted Microencapsulated Phase Change Material with Enhanced Thermo-Physical Properties and Photo-Thermal Performance. *Sol. Energy Mater. Sol. Cells* **2015**, *143*, 29−37.
(25) Dao, T. D.; Jeong, H. M. A Pickering Emulsion Route to A Stearic Acid/Graphene Core-Shell Composite Phase Change Material. *Carbon* **2016**, *99*, 49−57.
(26) Zhang, Y.; Zheng, X. H.; Wang, H. T.; Du, Q. G. Encapsulated Phase Change Materials Stabilized by Modified Graphene Oxide. *J. Mater. Chem. A* **2014**, *2*, 5304−5314.
(27) Ashby, N. P.; Binks, B. P. Pickering Emulsions Stabilised by Laponite Clay Particles. *Phys. Chem. Chem. Phys.* **2000**, *2*, 5640−5646.
(28) Ferrari, A. C.; Basko, D. M. Raman Spectroscopy as a Versatile Tool for Studying the Properties of Graphene. *Nat. Nanotechnol.* **2013**, *8*, 235−246.
(29) Camp, C. H., Jr; Cicerone, M. T. Chemically Sensitive Bioimaging with Coherent Raman Scattering. *Nat. Photonics* **2015**, *9*, 295−305.
(30) Rao, A. M.; Eklund, P. C.; Bandow, S.; Thess, A.; Smalley, R. E. Evidence for Charge Transfer in Doped Carbon Nanotube Bundles from Raman Scattering. *Nature* **1997**, *388*, 257−259.
(31) Cheng, C.; Li, D. Solvated Graphenes: An Emerging Class of Functional Soft Materials. *Adv. Mater.* **2013**, *25*, 13−30.
(32) Li, Y. L.; Yang, J.; Zhao, Q. H.; Li, Y. Dispersing Carbon-Based Nanomaterials in Aqueous Phase by Graphene Oxides. *Langmuir* **2013**, *29*, 13527−13534.
(33) Lee, H. S.; Yun, C. H.; Kim, H. M.; Lee, C. J. Persistence Length of Multiwalled Carbon Nanotubes with Static Bending. *J. Phys. Chem. C* **2007**, *111*, 18882−18887.
(34) Cerda, E.; Mahadevan, L. Geometry and Physics of Wrinkling. *Phys. Rev. Lett.* **2003**, *90*, 074302.
(35) Suk, J. W.; Piner, R. D.; An, J.; Ruoff, R. S. Mechanical Properties of Monolayer Graphene Oxide. *ACS Nano* **2010**, *4*, 6557−6564.
(36) Lee, C.; Wei, X.; Kysar, J. W.; Hone, J. Measurement of the Elastic Properties and Intrinsic Strength of Monolayer Graphene. *Science* **2008**, *321*, 385−388.
(37) Landau, L. D.; Pitaevskii, L. P.; Kosevich, A. M.; Lifshitz, E. M.:\ *Theory of Elasticity*; Elsevier Science, 2012.
(38) Seydou, M.; Marsaudon, S.; Buchoux, J.; Aimé, J. P.; Bonnot, A. M. Molecular Mechanics Investigations of Carbon Nanotube and Graphene Sheet Interaction. *Phys. Rev. B: Condens. Matter Mater. Phys.* **2009**, *80*, 245421.
(39) Yu, A.; Ramesh, P.; Sun, X.; Bekyarova, E.; Itkis, M. E.; Haddon, R. C. Enhanced Thermal Conductivity in a Hybrid Graphite Nanoplatelet − Carbon Nanotube Filler for Epoxy Composites. *Adv. Mater.* **2008**, *20*, 4740−4744.
(40) Lakkaraju, S. K.; Hwang, W. Critical Buckling Length *versus* Persistence Length: What Governs Biofilament Conformation? *Phys. Rev. Lett.* **2009**, *102*, 118102.
(41) Samanta, S. K.; Fritsch, M.; Scherf, U.; Gomulya, W.; Bisri, S. Z.; Loi, M. A. Conjugated Polymer-Assisted Dispersion of Single-Wall Carbon Nanotubes: The Power of Polymer Wrapping. *Acc. Chem. Res.* **2014**, *47*, 2446−2456.
(42) Grossiord, N.; Loos, J.; Regev, O.; Koning, C. E. Toolbox for Dispersing Carbon Nanotubes into Polymers to Get Conductive Nanocomposites. *Chem. Mater.* **2006**, *18*, 1089−1099.
(43) Sharma, A.; Tyagi, V. V.; Chen, C. R.; Buddhi, D. Review on Thermal Energy Storage with Phase Change Materials and Applications. *Renewable Sustainable Energy Rev.* **2009**, *13*, 318−345.
(44) Gunther, E.; Mehling, H.; Hiebler, S. Modeling of Subcooling and Solidification of Phase Change Materials. *Modell. Simul. Mater. Sci. Eng.* **2007**, *15*, 879−892.
(45) Huxtable, S. T.; Cahill, D. G.; Shenogin, S.; Xue, L.; Ozisik, R.; Barone, P.; Usrey, M.; Strano, M. S.; Siddons, G.; Shim, M.; Keblinski, P. Interfacial Heat Flow in Carbon Nanotube Suspensions. *Nat. Mater.* **2003**, *2*, 731−734.
(46) Swartz, E. T.; Pohl, R. O. Thermal-Boundary Resistance. *Rev. Mod. Phys.* **1989**, *61*, 605−668.
(47) Song, X. H.; Yang, Y. F.; Liu, J. C.; Zhao, H. Y. PS Colloidal Particles Stabilized by Graphene Oxide. *Langmuir* **2011**, *27*, 1186−1191.
(48) Liu, Z. P.; Zou, R. Q.; Lin, Z. Q.; Gui, X. C.; Chen, R. J.; Lin, J. H.; Shang, Y. Y.; Cao, A. Y. Tailoring Carbon Nanotube Density for Modulating Electro-to-Heat Conversion in Phase Change Composites. *Nano Lett.* **2013**, *13*, 4028−4035.
(49) Wang, S.; Tozaki, K.-i.; Hayashi, H.; Hosaka, S.; Inaba, H. Observation of Multiple Phase Transitions in *n*-C22H46 Using a High Resolution and Super-Sensitive DSC. *Thermochim. Acta* **2003**, *408*, 31−38.

DOI: 10.1021/acsnano.6b01104
ACS Nano 2016, 10, 4695−4703

(50) Fu, D.; Su, Y.; Xie, B.; Zhu, H.; Liu, G.; Wang, D. Phase Change Materials of *n*-Alkane-Containing Microcapsules: Observation of Coexistence of Ordered and Rotator Phases. *Phys. Chem. Chem. Phys.* **2011**, *13*, 2021−2026.

DOI: 10.1021/acsnano.6b01104
ACS Nano 2016, 10, 4695−4703